Ceramics International 49 (2023) 38015–38025

Contents lists available at ScienceDirect

Ceramics International

journal homepage: www.elsevier.com/locate/ceramint

A characteristic map as an approach for rapid estimating the thermal conductivity of high-temperature oxide ceramics demonstrated on 10Sc1CeSZ

Aydan Gedik *, Jonas Hesse, Stephan Kabelac

Institute of Thermodynamics, Leibniz University Hannover, Welfengarten 1, Hannover, D-30167, Lower Saxony, Germany

ARTICLE INFO

Keywords:
Solid oxide fuel cell (SOFC)
High-temperature
Oxide ceramic
Heat conductivity
Thermal conductivity
Electrolyte
8YSZ
10Sc1CeSZ

ABSTRACT

This work presents an easy applicable method for estimating thermal conductivity of oxide ceramic samples in a high-temperature SOFC/SOEC system. An experimental investigation establishes a thermal conductivity map for various oxide ceramics in the temperature range of 700 - 900 °C. Material specific properties are determined using laser flash analysis, displacement measurement for density and differential scanning calorimetry for heat capacity. The total thermal conductivity, incorporating conduction and radiation, is assumed based on a linear relationship with temperature gradient. Deviations in measurements are attributed to increasing radiation effects. The method provides a rough estimation of thermal conductivity, with 8YSZ exhibiting good agreement with literature values and 10Sc1CeSZ showing a range of 2.3 (+0.32/-0.48) - 2.8 (+0.96/-1) W/mK.

1. Introduction

A reliable quantitative description of the heat, mass and charge transport mechanisms occurring in solid oxide fuel cells (SOFC) is relevant for cell development and the optimisation of operating strategies. The performance and lifetime of a SOFC are determined by large temporal and spatial temperature gradients. Zeng et al. show that excessive temperature gradients in SOFCs can lead to delamination and cracks in the electrolyte and electrode materials [1]. Two types of heat generation are important. "Reversible" heat is due to the reaction entropies which have to be supplied or removed at the cathode and the anode, while irreversible heat is caused by dissipated energy. Dissipated energy is caused by ohmic resistances and overvoltages at the electrodes. In contrast, the electrochemical reaction at the three-phase interface leads to a thermoelectric effect in which reversible heat is released or absorbed at each electrode. Using the non-equilibrium thermodynamics (NET) approach, it is shown in a 1D model for a SOFC single cell with an 8YSZ electrolyte that a heat flux flows towards the temperature maximum near the cathode reaction layer, thus highlighting the importance of the Peltier effect [2]. The following NET-equation applies to the heat flow J_q^e in the electrolyte (e) [2]:

$$J_q^e = -\lambda^e \cdot \frac{dT}{dy} + \pi^e \cdot j, \tag{1}$$

where λ^e is the thermal conductivity, π^e is the Peltier coefficient of the electrolyte and j is the current density. As electrochemical reactions and the properties of the electrolyte, such as the ionic conductivity, are temperature-dependent, the knowledge of the thermal conductivity of the electrolyte is of great importance for a detailed analysis of the transport mechanisms and the resulting temperature distribution, cf. Eq. (1). Due to their lower thermal conductivity, oxide ceramic materials are also being investigated for their applications as thermal barrier coatings.

In the literature, yttria-stabilised zirconia (YSZ) and gadolinium-doped ceria (GDC) are described as the most commonly used electrolytes in electrochemical solid oxide applications. By adding aliovalent oxides, the cubic phase of zirconium oxide can be stabilised from room temperature to the melting point. Usually, calcium oxide (CaO), yttria (Y_2O_3), magnesia (MgO) and scandia (Sc_2O_3) are used for this purpose. The more similar the ionic radii of the substitution ions and the zirconium ion are, the higher is the ionic conductivity [3]. For YSZ in particular, a distinction is made between fully stabilised (FSZ, 8–12 mol%) and partially stabilised (PSZ, 3–5 mol%) zirconium oxide, with 8YSZ being the most widely used electrolyte for SOFCs. While PSZ has a higher mechanical load capacity, the ionic conductivity is reduced at the same time due to the lack of oxygen gaps. So raising the concentration of the dopant will raise the concentration of oxygen gaps. However, above a certain doping concentration, the gaps formed interact with each other and form associated centres, which in turn impair the mobility of the ions [4]. Accordingly, there are some studies

* Corresponding author.
E-mail address: gedik@ift.uni-hannover.de (A. Gedik).
URL: https://www.ift.uni-hannover.de/de/gedik/ (A. Gedik).

https://doi.org/10.1016/j.ceramint.2023.09.132
Received 16 June 2023; Received in revised form 1 September 2023; Accepted 13 September 2023
Available online 18 September 2023

on a combination of PSZ and FSZ to combine mechanical stability and ionic conduction [5].

At lower temperatures (600–700 °C), Sc_2O_3 is used to stabilise the cubic phase, as this compound has a very high ionic conductivity. By additional doping with ceria (CeO_2), a phase transformation below 650 °C can be prevented. From these findings, a combination of 10 mol% Sc_2O_3, which is necessary to stabilise the cubic phase, with a simultaneous maximum in the ionic conductivity [3] and 1 mol% CeO_2 is considered to be promising [5].

Numerous experimental studies on the electrical properties of YSZ and ScSZ can be found in the literature, whereas comparatively few experimental studies on 10Sc1CeSZ are available [6–11]. Specifically for the thermal conductivity of YSZ and ScSZ, the work of Schlichting et al. [12], Mévrel et al. [13], Fèvre et al. [14] and Sun et al. [15] should be highlighted. The ionic conductivity of 10Sc1CeSZ is still a current research topic [16–21], whereas only one study exists concerning the determination of thermal conductivity [22]. Their measurement is only carried out in the temperature range from 50–300 K.

CeO_2 is usually doped with other oxides of lanthanides. The most common compound is GDC or samarium oxide (SDC), as these compounds have the highest ionic conductivities [4]. Doped ceria is mainly used at lower temperatures (550 °C) due to its higher ionic conductivity and lower activation energy compared to stabilised zirconium oxide. Doped ceria is used especially for SOFCs that are operated with methanol. It can also be used as a coating for the boundary layer between electrolyte and electrode [3,4,23,24].

The accurate determination of the thermal conductivity of oxide ceramics is a great challenge, especially at the high operating temperatures (600–1000 °C). The simplest measurement is made according to Fourier's law via the measurement of a temperature gradient $\mathrm{d}T$ generated by a constant heat flow $\dot{Q}$ through a geometry with a surface A and thickness d:

$$\dot{Q} = -\lambda \cdot \frac{A}{d} \cdot \mathrm{d}T. \tag{2}$$

Cahill et al. [25] describes some problems of this method when performed at temperatures deviating from room temperature and describes the 3 ω-method as a promising technique for direct thermal conductivity measurement, especially as this method shows immunity to radiation errors at temperatures up to 1000 K. The most common and probably simplest method is the indirect measurement of thermal conductivity via the thermal diffusivity a, density ρ and specific heat capacity c of the material according to the following equation:

$$\lambda = a \cdot \rho \cdot c. \tag{3}$$

The thermal diffusivity can be determined using the laser flash method (LFM), the specific heat capacity using differential scanning calorimetry (DSC) and the density using a pycnometer. For a quick estimation method, however, both the direct method and the indirect method prove to be laborious, time-consuming and expensive.

In the present study, therefore, an attempt is made to create a characteristic diagram that is as generally valid as possible in the temperature range of 700–900 °C by experimentally investigating various well known oxide ceramic materials (Al_2O_3, ATi, ATZ, ZTA, Y_2O_3, 3YSZ). This thermal conductivity map is to be used for quick classification of future oxide ceramic materials that have not been investigated before. In this new methodology, the measured thermal conductivities of known oxide ceramic samples are plotted as a function of an imposed heat flux and their temperature difference, so that the thermal conductivity of an unknown sample can be interpolated by these dependencies between known values. The measurements are based exclusively on macroscopic methods. This methodology is first verified using 8YSZ, since, as mentioned above, some studies on the thermal conductivity of 8YSZ exist in the literature. Subsequently, the thermal conductivity of 10Sc1CeSZ is estimated to be able to simulate the processes taking place in the cell and the operating behaviour using the 1D NET SOFC model.

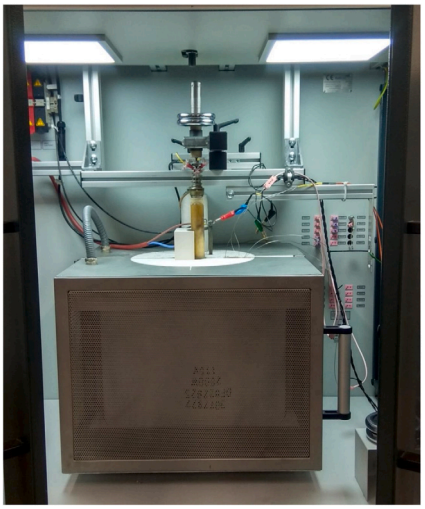

Fig. 1. Test room of the SOFC/SOEC test bench (Evaluator C1000-HT).

2. Material and methods

2.1. Test environment

For the development of a thermal conductivity map for different oxide ceramic electrolytes, the temperature difference $\mathrm{d}T$ is measured at different temperature levels (700–900 °C) over an oxide ceramic sample (40 × 40 × 10 mm) and a map is developed by linking these temperature differences with the predetermined thermal conductivities of the reference samples. For this purpose, a SOFC/SOEC test bench (Evaluator C1000-HT) from HORIBA FuelCon is available, which is suitable for the investigation of individual components, cf. Fig. 1. The central element of the test chamber is a hinged furnace in which the actual measuring chamber is located, cf. Fig. 2. A ceramic HT tube heater from Rauschert (110 VAC/480 W) is used to apply a heat flux to the sample. The Inconel block distributes the heat of the trace heater evenly over the entire surface due to its high thermal conductivity. The power of the tube heater can be controlled between 0–100% (equivalent to 30 W) and measured via a Digalox DPM72-MP+ power measurement sensor from TDE Instruments (±1% TRMS). For the characterisation of the measuring chamber, the absolute temperature measurement is carried out via several type-N thermocouples. The direct measurement of the temperature difference is carried out by connecting two type-S thermocouples with opposite poles. These thermocouples are placed on top and at the bottom of the sample and are calibrated with the high temperature calibrator Pegasus 4853 from ISOTECH. The GUM and DIN EN 60584-1 are used to determine the measurement uncertainty and the limit deviation.

2.2. Oxide ceramic samples

For the experimental investigation, a selection of some ceramic materials is made on the basis of a literature study in which material-typical characteristic values are to be obtained as first reference values. The selection is intended to cover a wide spectrum of oxide ceramics with various thermal conductivities, so that based on this, a characteristic diagram can be created that is as generally valid as possible. Since some materials or material compositions are similar in their behaviour, the number of oxide ceramics to be investigated will be reduced to 6, see Fig. 3 and Table 1. The selected oxide ceramics are first examined with regarding their own thermal conductivity. The thermal diffusivity a, the density ρ and the heat capacity c_p are being determined according to Eq. (3) for this purpose.

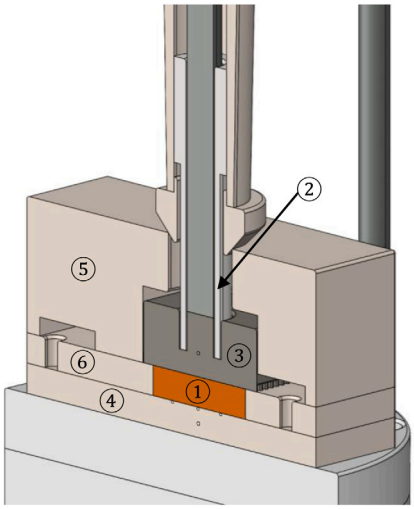

Fig. 2. Measuring chamber (1) Sample, (2) Tubular heater, (3) Inconel block with channels, (4) Kermam base plate with recesses, (5) Housing, (6) Sealing frame.

Table 1
Selected reference oxide ceramics.

Material	Structure	Manufacturer	ρ [g/cm^3]	λ at AT [W/m K]
Al_2O_3	99.7% Al_2O_3	TKC – Technische Keramik GmbH	3.9	30
ATi	Al_2TiO_5	ZELL QUARZGLAS	3.35	1.4
ATZ	20 mol % Al_2O_3 -doped ZrO_2	BCE Special Ceramics GmbH	5.4	6
ZTA	12 mol % ZrO_2 -doped Al_2O_3	BCE Special Ceramics GmbH	4.1	25
Y23	Y_2O_3	Friatec GmbH	4.9	8–12
3YSZ	3 mol % Y_2O_3 -doped ZrO_2	ZELL QUARZGLAS GmbH	6	2.5
8YSZ	8 mol % Y_2O_3 -doped ZrO_2	CerPoTec AS	N/A	N/A
10Sc1CeSZ	10 mol % Sc_2O_3 –1 mol % CeO_2 -doped ZrO_2	CerPoTec AS	N/A	N/A

3. Calculation/theory

3.1. Thermal diffusivity

For the experimental determination of the thermal diffusivity, two samples of the same material are coated with gold and/or graphite and characterised via laser flash analysis. The measurement is repeated 6 times at each measuring point (temperature). Fig. 4 shows that the thermal diffusivity of the samples generally decreases with increasing temperatures. Analogous to the thermal conductivity known from the literature, the ATi sample shows a different behaviour. In the temperature range considered, a sigmoid behaviour is shown. This behaviour is attributed to the self-healing of microcracks in the microstructure, which reduces the thermal resistance at the grain boundaries and consequently improves the conductive heat transport [27].

3.2. Density

The density is determined by volume displacement in a 10 ml pycnometer. Therefore, the samples, the empty pycnometer, the filled pycnometer and the filled pycnometer with sample are accurately weighed. From the mass difference of the known fluid (in this case deionised water) at a given temperature, the volume displaced by the sample can be determined, which is connected to the unknown density via the mass weight. Repeated measurements show that the manufacturer's specifications are confirmed within a maximum error interval of +/− 10%. However, it is noticeable that some measurements deviate positively from the manufacturer's specifications. Only negative deviations can be expected, since the material can only have a lower density than the theoretical density due to porosities or structural defects. Due to the very simplified methodology, the results are only used for comparison with the manufacturer's specifications.

3.3. Heat capacity

3.3.1. Theoretical approaches

The simplest method for estimating heat capacities at 298.15 K is the Neumann–Kopp rule established in 1865. According to Eq. (4), the specific heat capacities $C_{p,i}^{\Theta}$ of the individual components i of the molecule under consideration are summed up with their respective mass fractions x_i:

$$C_p^{\Theta} = \sum_{i=1}^{N} x_i \cdot C_{p,i}^{\Theta} \tag{4}$$

where N is the total number of constituents of the molecule. The method is also applicable to the temperature dependence of the heat capacity $C_p(T)$. The first empirical method for estimating heat capacities of predominantly ionic compounds was established by H.H. Kellogg [30]. Based on experimental data of heat capacities at 298.15 K, he estimated the individual contributions of cations and anions for molecules. Another similar method is the Mostafa et al. method, in which the heat capacity at 298.15 K is calculated by contributions from individual ions or functional groups in a molecule [31]. Kubaschewski and Ünal [32] extended H.H. Kellogg's methodology on the basis that the heat capacity of individual ions or atoms is the same at the melting point and formulated the following temperature-dependent equations:

$$C_p(T) = A + B \cdot T + \frac{C}{T^2} \tag{5}$$

with the parameters

$$A = \frac{10^{-3} \cdot T_m\,[C_p^{\Theta}(298.15\,\mathrm{K}) + 4.7\,n] - 1.25\,n \cdot 10^{-5}(T_m)^{-2} - 9.05\,n}{10^{-3} \cdot T_m - 0.298}$$
$$B = \frac{25.6\,n + 4.2\,n \cdot 10^{-5}(T_m)^{-2} - C_p^{\Theta}(298.15\,\mathrm{K})}{10^{-3} \cdot T_m - 0.298} \tag{6}$$
$$C = -4.2\,n$$

with T_m as the melting temperature and n as the total number of atoms of the molecule (for Al_2O_3 applies n = 5). The approach only applies to substances with a melting temperature below 2300 K. Another estimation method for determining the temperature-dependent heat capacity of solid oxides is the Berman and Brown method, which, however, only applies to selected binary oxides:

$$C_p = k_0 + \frac{k_1}{T^{1/2}} + \frac{k_2}{T^2} + \frac{k_3}{T^3}. \tag{7}$$

The parameters k_0, k_1, k_2 and k_3 for the oxides can be found in [33]. In their studies, Leitner et al. [34,35] compare the different methods with experimental data. They show that Mostafa's method yields a mean error of 4.27% for 92 oxides, Neumann–Kopp rule a mean error of 3.3% for more than 74 oxides and Kellogg a mean error of 3.1% for 169 oxides. Wang et al. [36] also show that Mostafa's methodology performs worse compared to the Neumann–Kopp rule and Kubaschewski and Ünal method. For the compounds of the Berman and Brown method, a mean error of 1.5% is calculated, which is within a typical error range of a DSC measurement (1–3%). Accordingly, the methods are well suited for making initial estimates regarding heat capacities.

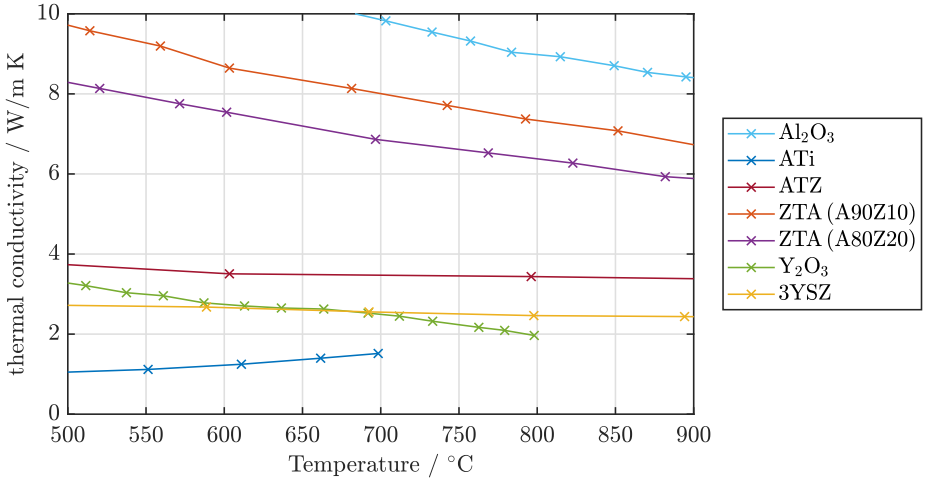

Fig. 3. Literature values for thermal conductivity λ as a function of temperature T for various oxide ceramics (Al_2O_3 [26], ATi [27], ATZ [28], ZTA [28], Y_2O_3 [29], 3YSZ [12]).

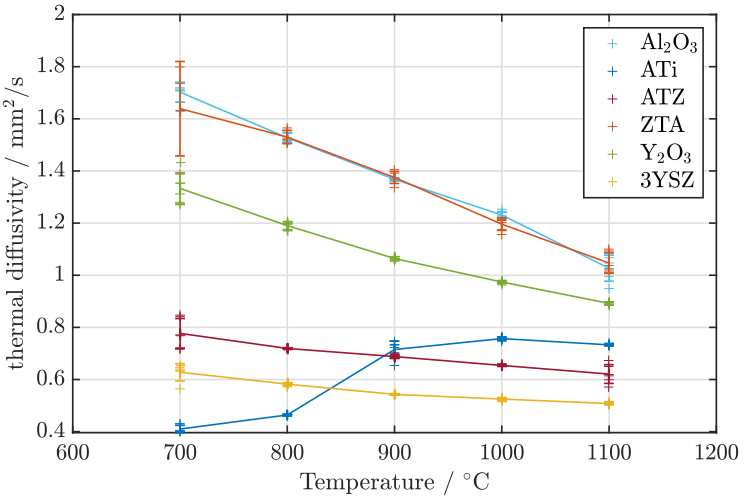

Fig. 4. Measured temperature diffusivities a as a function of temperature T for the selected oxide ceramics using LFM.

The results for heat capacities of Al_2O_3, ATi, ATZ, ZTA, Y_2O_3 and 3YSZ are shown in Fig. 5. As the melting points of Al_2O_3 and Y_2O_3 are higher than 2300 K, there are deviations in the approach of Kubaschewski and Ünal. In the relevant range of 600–1000 °C the determined data show a uniform behaviour. Since neither the Berman & Brown method nor NIST data for Y_2O_3 are available, experimental data from the literature were used, which show deviations of up to 7% between them. For the further course of the analysis, the arithmetic mean is formed from this data.

3.3.2. Experimental determination

To enable a comparison of the theoretical values with real experimental data, a dynamic power compensation differential scanning calorimetry is carried out with a DSC 7 from PerkinElmer. In a temperature range of 100–550 °C, the heat flow into the sample is detected at a heating rate of 20 K/min, and can then be converted into a heat capacity by an appropriate program. The baseline is first configured and the temperature range is calibrated by the melting points of indium, bismuth and zinc. As described in DIN EN ISO 11357-4, a sapphire disc (α-aluminium oxide) serves as the reference material. The heat capacities of the selected oxide ceramic samples averaged from two measurements are plotted against temperature in 1 K increments in Fig. 6. In general, especially between 115–415 °C, a good agreement between measurement (lines) and the individual calculated quantities (points) is shown. In the last temperature range (415–550 °C), ATi and Y_2O_3 show a considerable deviation. Investigations suggest that the aluminium crucible expands particularly in this temperature range and a displacement of the platinum lid occurs. This results in heat losses, which are reflected in increased heat absorption. Thus these values have to be discarded.

3.4. Effective thermal conductivity

In Fig. 7 the thermal conductivity $\lambda(T)$ is calculated by Eq. (3) using the experimental values discussed above. It can generally be seen that the thermal conductivity $\lambda(T)$ behaves more strongly temperature-dependent in the low temperature range and less strongly temperature dependent in the high temperature range (>1000 °C). Most ceramic materials show a regressive behaviour of the thermal conductivity with increasing temperatures, as can also be observed for the thermal diffusivity, which is due to the phonon-dominated heat transport. The thermal conductivity of ATi increases degressively over the course of the temperature, as was also observed in the previous studies. Taking into account all the variables investigated, it can be stated that the thermal diffusivity is formative for the course of the thermal conductivity, since density and heat capacity are approximately constant over the temperature. It should be noted, however, that at high temperatures radiation effects must be taken into account, which improve the effective thermal conductivity. Manara et al. states that

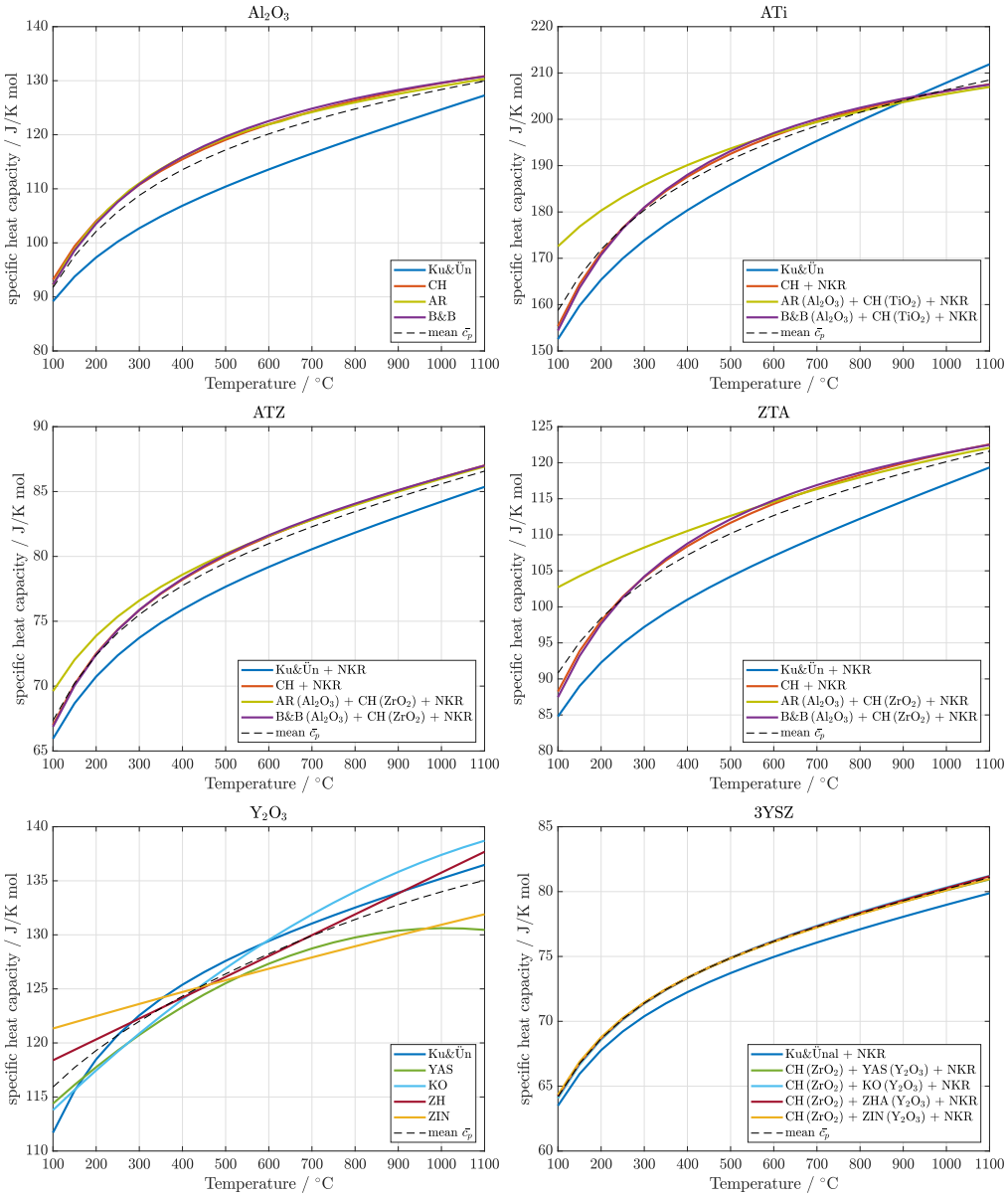

Fig. 5. Theoretically determined heat capacities C_p as a function of temperature T for the selected oxide ceramics (Ku&Ün: [32], CH: [37], AR: [38], B&B: [33], NKR: [35], YAS: [39], KO: [40], ZH: [41], ZIN: [42]).

radiative heat transfer becomes more important above 400 °C [43]. According to this, a total thermal conductivity applies [44]:

$$\lambda_{\text{total}} = \lambda_{\text{solid}} + \lambda_{\text{rad}}. \tag{8}$$

Further literature research shows that in the relevant infrared wavelength range of 1–7 μm, ceramic materials exhibit a temperature-dependent semitransparent behaviour, and thus more detailed investigations must be carried out regarding the radiation transport in oxide ceramics [43,45–49]. Manara et al. investigates the total heat transport through an Al_2O_3 and a PSZ (5.2 wt%) plate, taking into account the radiation-optical properties [44]. They calculate the effective thermal conductivity and splits this according to Eq. (8) into a thermal conductivity and radiation component. At 900 °C, this results in a maximum radiation component of 15% of the effective thermal conductivity. Because the radiation-optical properties of the materials are different, there is a need for such investigations. However, this project in particular will not go into it further details for the time being, we consider our thermal conductivity to be an effective one. According to Fourier's law, in the stationary one-dimensional case, heat conduction through a solid is given by:

$$q_{\text{solid}} = -\lambda \cdot \mathrm{d}T/\mathrm{d}x = -\frac{\lambda}{d} \cdot (T_2 - T_1) \text{ with } \mathrm{d}T/\mathrm{d}x = \text{const.} \tag{9}$$

From this relationship, the relationship between thermal conductivity and temperature gradient is used for the thermal conductivity map, which is the aim of this section:

$$\lambda \sim \frac{1}{T_2 - T_1}. \tag{10}$$

3.5. Experimental design

The measurements provide data in a temperature window between 700–900 °C in 50 K intervals. The power of the HT tube heater is varied between 0–100% in 25% (≙ 7 W) intervals per measurement. In order to avoid thermally induced mechanical stresses in the electrolyte, only

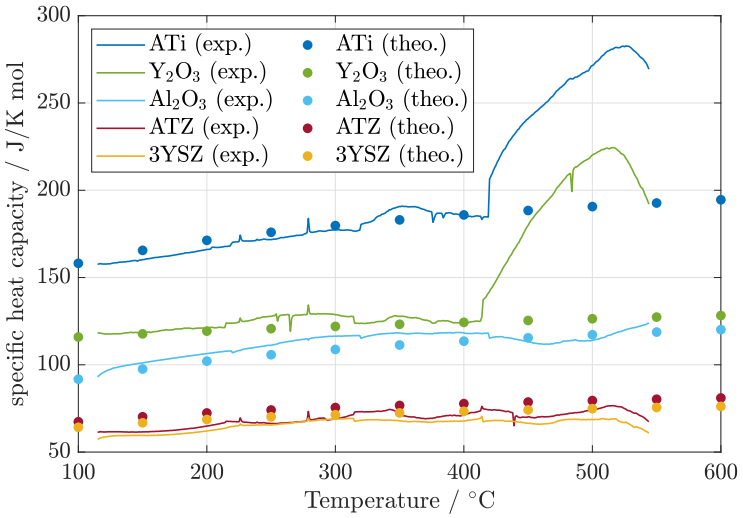

Fig. 6. Experimentally determined heat capacity.

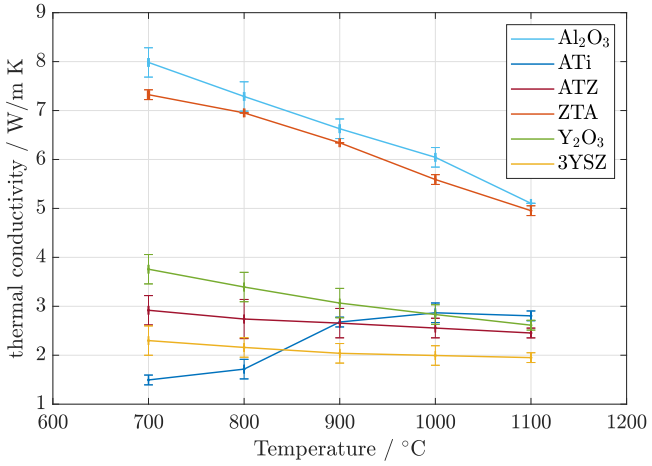

Fig. 7. Experimentally determined effective thermal conductivity.

slow changes in heating power are used. The test matrix is shown in Table 2. From the known thermal conductivities (cf. Fig. 7) and the measured temperature differences, a characteristic diagram is created as explained in Section 2. Then 8YSZ and 10Sc1CeSZ are measured and the unknown thermal conductivity is estimated with the help of the map. To ensure reproducibility, each sample was measured three times.

4. Results and discussion

4.1. Thermal conductivity map for different temperatures

The thermal conductivities of the samples are shown as a function of the measured temperature difference and the applied heating power for the furnace temperatures 700 °C and 900 °C in Fig. 8. Instead of the previously expected linear relationship, an exponential relationship between the thermal conductivity and the temperature difference is shown. However, it is important to note that this relationship only applies in this case where the total effective thermal conductivity is considered. This again underlines the importance of thermal radiation in heat transfer. Another factor that can influence heat transfer experiments is the thermal expansion of the various materials. When the sample expands due to heat input, it may come into contact with some surrounding components (especially the sealing frame) and transfer heat to them, which can lead to a distortion of the temperature

Table 2
Test matrix for the development of the thermal conductivity maps.

Parameter		Electrolyte							
ϑ	P_{HTth}	Al_2O_3	ATi	ATZ	ZTA	Y_2O_3	3YSZ	8YSZ	10Sc1CeSZ
700 °C	0%								
⋮	⋮					⋮			
⋮	⋮					⋮			
900 °C	⋮					⋮			
	100%								

difference. The thermal conductivity of a sample remains the same within a constant oven temperature. If the power of the HT tube heater is increased, the temperature difference increases linearly according to Fourier's law. The slope of the temperature difference depends on the thermal conductivity of the material – the lower the thermal conductivity, the higher the slope. In the temperature range from 700–900 °C, measurements show deviations, with higher deviations found at 900 °C than at 700 °C. This is because radiation effects are more relevant at higher temperatures. In addition, it can be seen that for the same electric power of the HT tube heater, lower temperature differences occur at higher furnace temperatures. Based on the resistance of the HT tube heater increases with temperature, resulting in lower heating power at higher furnace temperatures. At 700 °C the maximum power of the trace heater is 30 W, while at 900 °C it is only 26 W.

4.2. Exemplary determination of the effective thermal conductivities λ of 8YSZ and 10Sc1CeSZ for the temperature $T = 700$ °C

The following is an example of how the effective thermal conductivities of 8YSZ and 10Sc1CeSZ were determined by use of the interpolation map given in Fig. 8(a) for 700 °C. Fig. 9 shows the course of the thermal conductivities of all samples as a function of the measured temperature difference for each individual heating power. The expected results show significant temperature differences for the samples of 8YSZ and 10Sc1CeSZ, which are due to their low thermal conductivities. As mentioned in the introduction, high ionic conductivity in oxide ceramics is associated with low thermal conductivity. As expected, 10Sc1CeSZ is found to have a larger change in temperature difference with increasing heating power, indicating a higher slope of temperature difference compared to 8YSZ, which in turn indicates lower thermal conductivity. Other possible of influence factors could be the different optical properties of the samples and inaccuracies of the sensors. From the deviations of the measured temperature differences,

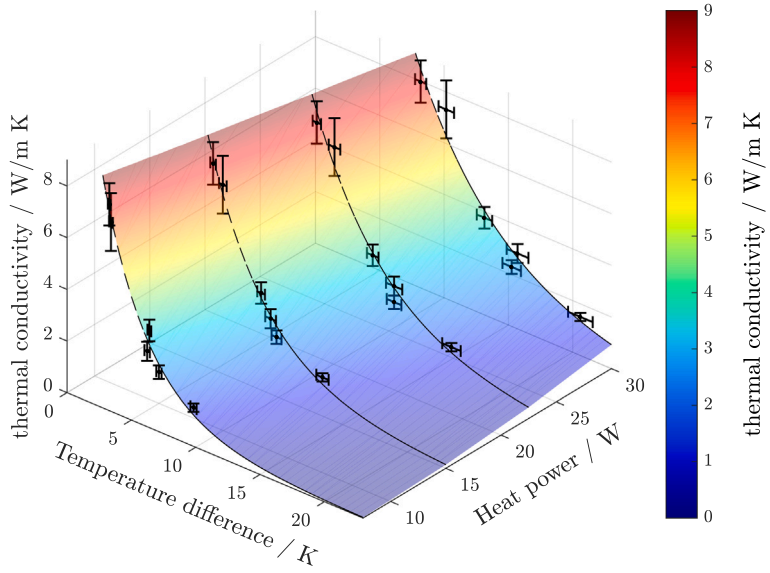

(a) Effective thermal conductivity λ as a function of temperature difference ΔT and applied heating power $\dot{Q}$ for a temperature of 700 °C

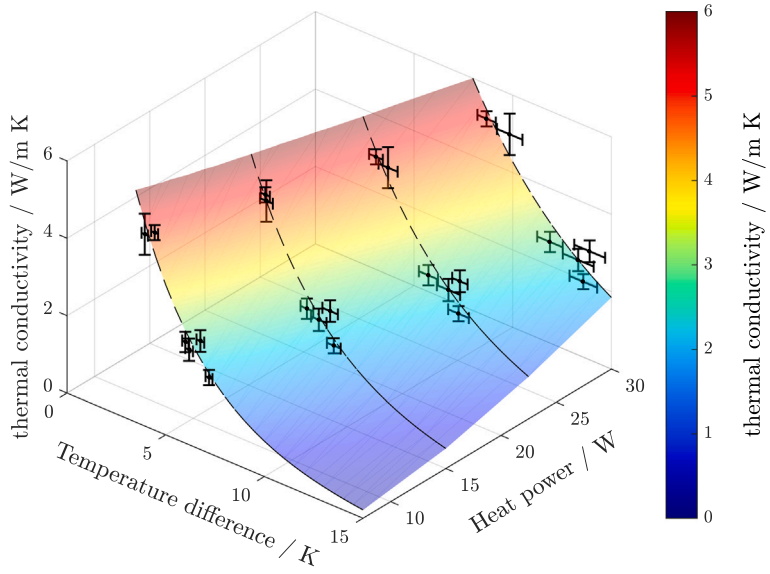

(b) Effective thermal conductivity λ as a function of temperature difference ΔT and applied heating power $\dot{Q}$ for a temperature of 900 °C

Fig. 8. Measured thermal conductivity map for a temperature of 700 °C and 900 °C.

the deviations of the effective thermal conductivities for 8YSZ and 10Sc1CeSZ can be determined with the help of the fitting curves. The individual interpolated values are then compiled in a diagram, cf. Fig. 10. Ideally, the same thermal conductivity should be determined within a material for each heating power, and thus for each temperature difference. However, it can be seen that with increasing heating power, the thermal conductivity of 8YSZ increases slightly, while it decreases slightly for 10Sc1CeSZ. It is important to note that the values were determined based on the curve of all measurements including their measurement deviations. However, these deviations are within the acceptable range. Therefore, an average value for each sample at one oven temperature is determined from the determined values in Fig. 10. This process is repeated for the oven temperature data from 750–900 °C.

4.3. Determination of the effective thermal conductivities λ of 8YSZ and 10Sc1CeSZ for a temperature of 700–900 °C

The results are shown in Fig. 11. For direct comparison, the known values from the literature are implemented as well. The thermal conductivity values of 8YSZ determined in this study show good agreement with literature values. The largest deviations occur in the values for 850 °C and 900 °C, which can be attributed to the influences of radiation. Based on this first assessment, it can be stated that the thermal conductivity of a sample can be well approximated by the maps proposed in this work. The analysis of the maps show a thermal conductivity of 2.3 (+0.32/−0.48)–2.8 (+0.96/−1) W/mK for 10Sc1CeSZ in the temperature range from 700–900 °C. Similar to 8YSZ, there was an outlier value at 900 °C, so a more realistic range of 2.2

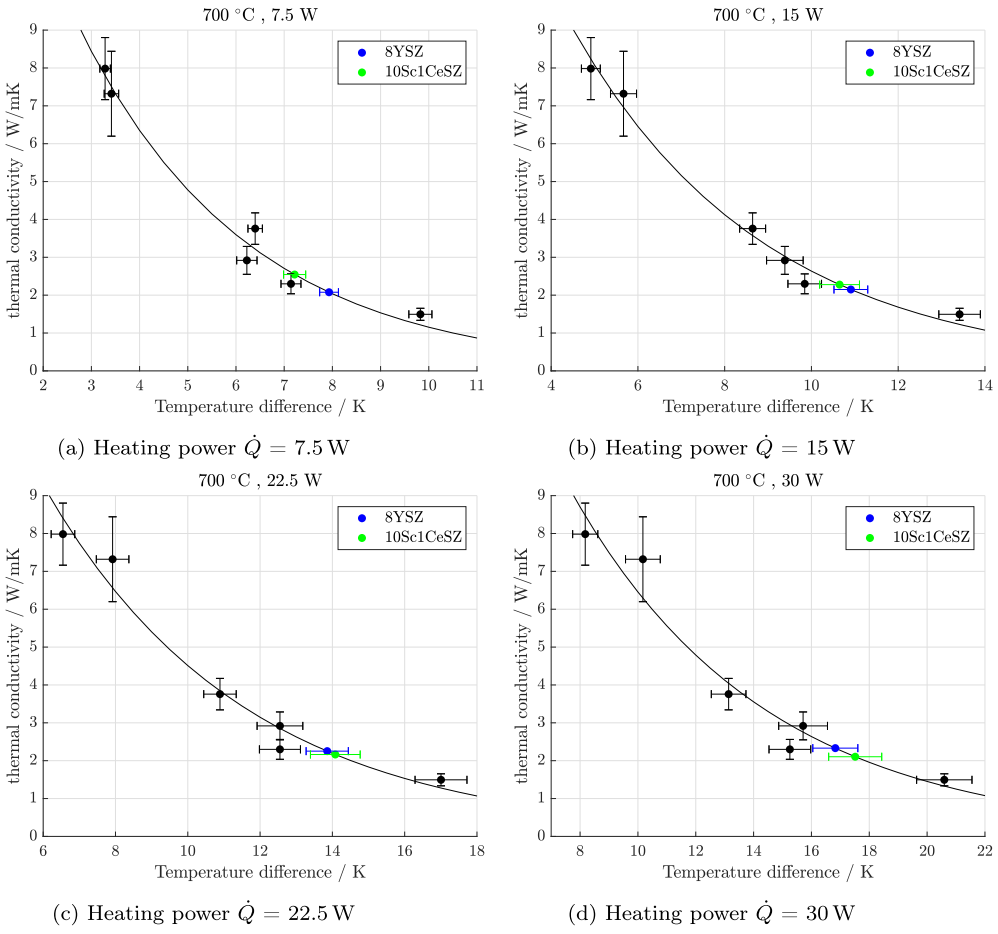

(a) Heating power $\dot{Q} = 7.5\,\mathrm{W}$ (b) Heating power $\dot{Q} = 15\,\mathrm{W}$

(c) Heating power $\dot{Q} = 22.5\,\mathrm{W}$ (d) Heating power $\dot{Q} = 30\,\mathrm{W}$

Fig. 9. Effective thermal conductivity λ as a function of temperature difference ΔT divided into the heating power $\dot{Q}$ for a temperature of 700 °C.

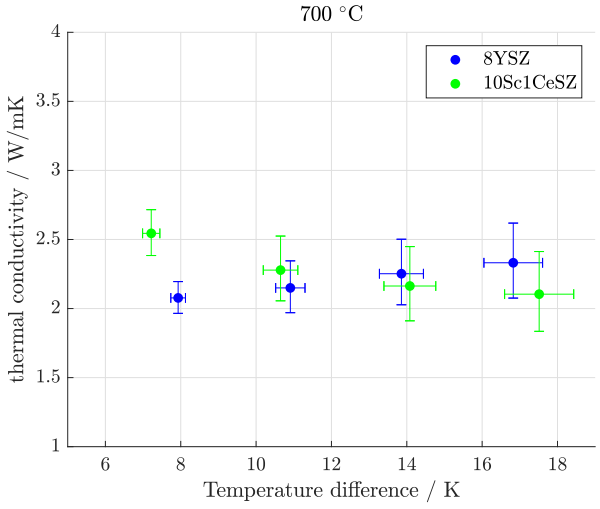

Fig. 10. Interpolated effective thermal conductivity λ of 8YSZ and 10Sc1CeSZ as a function of temperature difference ΔT for all heating powers $\dot{Q}$ for a temperature of 700 °C.

(+0.41/−0.24)–1.68 (+0.42/−0.26) W/mK was found. Based on the previously mentioned relationship between ionic conductivity and thermal conductivity, a thermal conductivity of 10Sc1CeSZ lower than 8YSZ should have resulted, as expected, since the ionic conductivity of 8YSZ is lower than that of 10Sc1CeSZ, cf. [50–52]. Furthermore, it must be assumed that the actual thermal conductivities are lower than the measured effective thermal conductivities, as this increase is due to radiation effects. Entered in the thermal conductivity map for a heating power of 30 W as a function of the different operating temperatures, the deviations with regard to higher temperatures are once again made clear, cf. Fig. 12.

5. Conclusion

In this work, an experimental interpolation is developed to estimate the thermal conductivity of oxide ceramic samples for potential SOFC/SOEC applications at high temperatures. Accurate determination of thermal conductivity in this temperature range is usually laborious, time consuming and expensive. Therefore, an experimental investigation is conducted to establish a thermal conductivity map for various oxide ceramic samples in the temperature range of 700–900 °C as a basis for interpolation. An electrical heating current is imposed and the temperature difference is measured, so this data can then be subsequently compared to the known values in the map. To prepare this map, the material-specific properties of thermal diffusivity, density and specific heat capacity of the selected materials are determined. For this purpose, laser flash analysis, displacement measurement, and differential scanning calorimetry are performed. These results are compared with manufacturer and literature data and converted into a thermal conductivity by multiplication. This is followed by a series of measurements in the range 700–900 °C in 50 K increments using an electric heater to determine the temperature difference across a 10 mm thick oxide ceramic block.

Since radiation effects must be considered at high temperatures, a total effective thermal conductivity is assumed to include both conduction and radiation. The different optical properties of the materials are

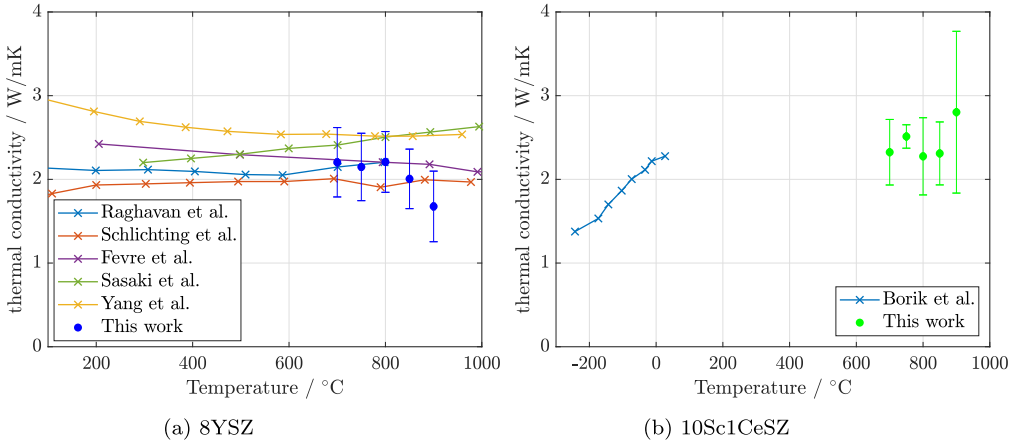

Fig. 11. Comparison of the interpolated effective thermal conductivities λ with data from the literature (RA: [53], SCH: [12], FE: [14], SA: [54], YA: [55], BO: [22]).

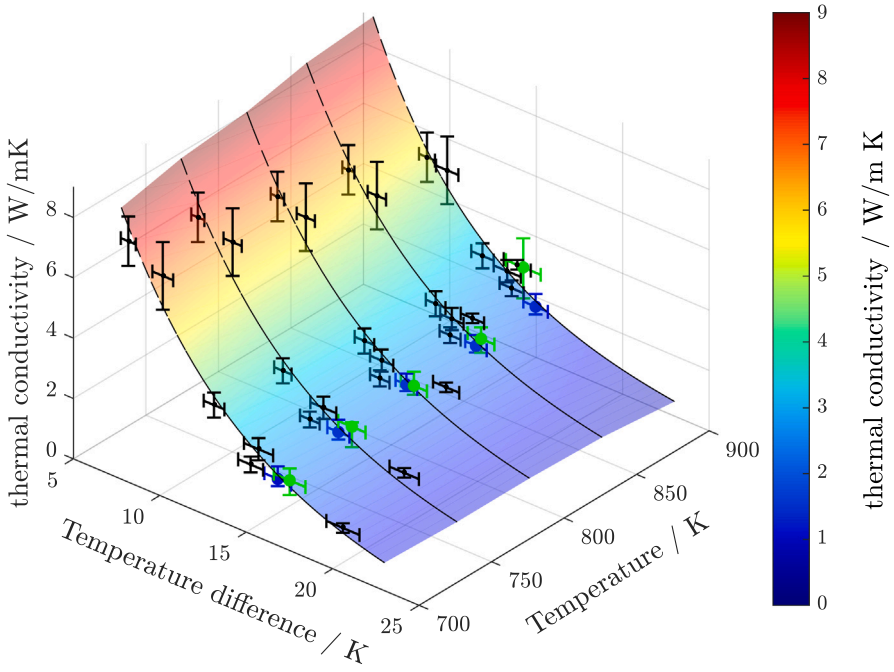

Fig. 12. Measured thermal conductivity map: Effective thermal conductivity λ as a function of temperature difference ΔT and temperature for a applied heating power $\dot{Q}$ of 30 W.

not initially elaborated and considered in this work. A direct linear relationship is assumed between the total thermal conductivity and the temperature gradient at an operating temperature. However, an exponential relationship over different operating temperatures shows the importance of thermal radiation in heat transfer. Also, increasing deviations in the temperature difference measurements in the results show the importance of increasing radiation effects as temperature increases. Furthermore, the increase of the temperature leads to the increase of the resistance of the HT tube heater, so that accordingly the electrical heating conduction decreases and the temperature differences decrease. The effective thermal conductivity of 8YSZ determined using the recorded map as a test shows good overall agreement with literature values at 2.2 (+0.41/−0.24)–1.68 (+0.42/−0.26) W/mK, although larger deviations are observed at 850 °C and 900 °C. For 10Sc1CeSZ as a second example, an interpolated effective thermal conductivity of 2.3 (+0.32/−0.48)–2.8 (+0.96/−1) W/mK results in the temperature range from 700–900 °C. It should be noted that the effective thermal conductivity is measured, so the actual solid-state thermal conductivity is lower. Overall, this method provides a rapid estimate of the thermal conductivity of oxide ceramic samples.

Declaration of competing interest

The authors declare that they have no known competing financial interests or personal relationships that could have appeared to influence the work reported in this paper.

Acknowledgments

The Deutsche Forschungsgemeinschaft (DFG) provided the experimental setup and materials as part of the major research instrumentation programm with contract number INST 187/630-1 FUGG. We would like to thank the Uni Bremen Campus GmbH (UBC) - Centre for Ceramic Materials for measuring the thermal diffusivity of the samples.

Funding

The authors gratefully acknowledge the financial support by the Deutsche Forschungsgemeinschaft (DFG, funding code KA 1211/32-1 and KA 1211/32-2) for financial support.

References

[1] Z. Zeng, Y. Qian, Y. Zhang, C. Hao, D. Dan, W. Zhuge, A review of heat transfer and thermal management methods for temperature gradient reduction in solid oxide fuel cell (SOFC) stacks, Appl. Energy (ISSN: 03062619) 280 (2020) 115899, http://dx.doi.org/10.1016/j.apenergy.2020.115899.

[2] A. Gedik, N. Lubos, S. Kabelac, Coupled transport effects in solid oxide fuel cell modeling, Entropy 24 (2) (2022) http://dx.doi.org/10.3390/e24020224.

[3] Q.M. Nguyen, T. Takahashi, Science and Technology of Ceramic Fuel Cells, Elsevier Science, Amsterdam and New York, 1995.

[4] R.P. O'Hayre, S.-W. Cha, W.G. Colella, F.B. Prinz, Fuel cell fundamentals, John Wiley & Sons Inc, Hoboken, New Jersey, 2016.

[5] Y. Brodnikovskyi, N. McDonald, I. Polishko, D. Brodnikovskyi, I. Brodnikovska, M. Brychevskyi, L. Kovalenko, O. Vasylyev, A. Belous, R. Steinberger-Wilckens, Properties of 10Sc1CeSZ-3.5ysz(33-, 40-, 50-wt.%) composite ceramics for SOFC application, Mater. Today: Proc. (ISSN: 22147853) 6 (2019) 26–35, http://dx.doi.org/10.1016/j.matpr.2018.10.071.

[6] A. Zarkov, A. Stanulis, J. Sakaliuniene, S. Butkute, B. Abakeviciene, T. Salkus, S. Tautkus, A.F. Orliukas, S. Tamulevicius, A. Kareiva, On the synthesis of yttria-stabilized zirconia: a comparative study, J. Sol-Gel Sci. Technol. (ISSN: 0928-0707) 76 (2) (2015) 309–319, http://dx.doi.org/10.1007/s10971-015-3778-1.

[7] M.O. Curi, H.C. Ferraz, J. Furtado, A.R. Secchi, Dispersant effects on YSZ electrolyte characteristics for solid oxide fuel cells, Ceram. Int. (ISSN: 02728842) 41 (5) (2015) 6141–6148, http://dx.doi.org/10.1016/j.ceramint.2015.01.072.

[8] N. Masó, A.R. West, Electronic conductivity in yttria-stabilized zirconia under a small dc bias, Chem. Mater. (ISSN: 0897-4756) 27 (5) (2015) 1552–1558, http://dx.doi.org/10.1021/cm503957x.

[9] L. Yao, W. Liu, G. Ou, H. Nishijima, W. Pan, Phase stability and high conductivity of ScSZ nanofibers: effect of the crystallite size, J. Mater. Chem. A (ISSN: 2050-7488) 3 (20) (2015) 10795–10800, http://dx.doi.org/10.1039/c4ta06712f.

[10] J. Tao, A. Dong, J. Wang, The influence of microstructure and grain boundary on the electrical properties of scandia stabilized zirconia, Mater. Trans. (ISSN: 1345-9678) 54 (5) (2013) 825–832, http://dx.doi.org/10.2320/matertrans.M2012385.

[11] G.Y. Cho, Y.H. Lee, S.W. Hong, J. Bae, J. An, Y.B. Kim, S.W. Cha, High-performance thin film solid oxide fuel cells with scandia-stabilized zirconia (ScSZ) thin film electrolyte, Int. J. Hydrogen Energy (ISSN: 03603199) 40 (45) (2015) 15704–15708, http://dx.doi.org/10.1016/j.ijhydene.2015.09.124.

[12] K.W. Schlichting, N.P. Padture, P.G. Klemens, Thermal conductivity of dense and porous yttria-stabilized zirconia, J. Mater. Sci. (ISSN: 00222461) 36 (12) (2001) 3003–3010, http://dx.doi.org/10.1023/A:1017970924312.

[13] R. Mévrel, J.-C. Laizet, A. Azzopardi, B. Leclercq, M. Poulain, O. Lavigne, D. Demange, Thermal diffusivity and conductivity of $zr_1 - xy_xo_{2-x/2}$ (x=0, 0.084 and 0.179) single crystals, J. Eur. Ceram. Soc. (ISSN: 09552219) 24 (10–11) (2004) 3081–3089, http://dx.doi.org/10.1016/j.jeurceramsoc.2003.10.045.

[14] M. Fèvre, A. Finel, R. Caudron, R. Mévrel, Local order and thermal conductivity in yttria-stabilized zirconia. II. numerical and experimental investigations of thermal conductivity, Phys. Rev. B (ISSN: 1098-0121) 72 (10) (2005) http://dx.doi.org/10.1103/PhysRevB.72.104118.

[15] L. Sun, H. Guo, H. Peng, S. Gong, H. Xu, Influence of partial substitution of Sc_2O_3 with Gd_2O_3 on the phase stability and thermal conductivity of Sc_2O_3-doped ZrO_2, Ceram. Int. (ISSN: 02728842) 39 (3) (2013) 3447–3451, http://dx.doi.org/10.1016/j.ceramint.2012.09.100.

[16] I. Brodnikovska, N. Korsunska, L. Khomenkova, Y. Polishchuk, S. Lavoryk, M. Brychevskyi, Y. Brodnikovskyi, O. Vasylyev, Grains, grain boundaries and total ionic conductivity of 10Sc1CeSZ and 8YSZ solid electrolytes affected by crystalline structure and dopant content, Mater. Today: Proc. (ISSN: 22147853) 6 (2019) 79–85, http://dx.doi.org/10.1016/j.matpr.2018.10.078.

[17] I.V. Brodnikovska, Y.M. Brodnikovskyi, M.M. Brychevskyi, O.D. Vasylyev, Joint impedance spectroscopy analysis of 10Sc1CeSZ and 8YSZ solid electrolytes for SOFC, Powder Metall. Metal Ceram. (ISSN: 1068-1302) 57 (11–12) (2019) 723–730, http://dx.doi.org/10.1007/s11106-019-00037-4.

[18] I. Brodnikovska, N. Korsunska, L. Khomenkova, Y. Polishchuk, M. Brychevskyi, Y. Brodnikovskyi, D. Brodnikovskyi, I. Polishko, O. Vasylyev, The investigation of 10Sc1CeSZ structure transformation and ionic conductivity, Mater. Today: Proc. (ISSN: 22147853) 50 (2022) 487–491, http://dx.doi.org/10.1016/j.matpr.2021.11.299.

[19] D.A. Agarkov, M.A. Borik, S.I. Bredikhin, A.V. Kulebyakin, I.E. Kuritsyna, E.E. Lomonova, F.O. Milovich, V.A. Myzina, V.V. Osiko, E.A. Agarkova, N.Y. Tabachkova, Structure and transport properties of zirconia-based solid solution crystals co-doped with scandium and cerium oxides, Russ. J. Electrochem. (ISSN: 1023-1935) 54 (6) (2018) 459–463, http://dx.doi.org/10.1134/S1023193518060022.

[20] D.A. Agarkov, M.A. Borik, S.I. Bredikhin, I.N. Burmistrov, G.M. Eliseeva, V.A. Kolotygin, A.V. Kulebyakin, I.E. Kuritsyna, E.E. Lomonova, F.O. Milovich, V.A. Myzina, P.A. Ryabochkina, N. Tabachkova, T.V. Volkova, Structure and transport properties of zirconia crystals co-doped by scandia, ceria and yttria, J. Materiomics (ISSN: 23528478) 5 (2) (2019) 273–279, http://dx.doi.org/10.1016/j.jmat.2019.02.004.

[21] D. Agarkov, M. Borik, G. Eliseeva, A. Kulebyakin, E. Lomonova, F. Milovich, V. Myzina, Y. Parkhomenko, E. Skryleva, N. Tabachkova, Skull melting growth and characterization of $(ZrO_2)0.89(Sc_2O_3)0.1(CeO_2)0.01$ crystals, Crystals 10 (1) (2020) 49, http://dx.doi.org/10.3390/cryst10010049.

[22] M.A. Borik, A.V. Kulebyakin, I.E. Kuritsyna, E.E. Lomonova, V.A. Myzina, P.A. Popov, F.O. Milovich, N.Y. Tabachkova, Thermal conductivity of single-crystal ZrO_2-based solid solutions co-alloyed with scandium, cerium, and yttrium oxides, Phys. Solid State (ISSN: 1063-7834) 61 (12) (2019) 2397–2402, http://dx.doi.org/10.1134/S1063783419120060.

[23] M. Cassir, D. Jones, A. Ringuedé, V. Lair, Electrochemical devices for energy: fuel cells and electrolytic cells, in: Handbook of Membrane Reactors, Elsevier, 2013, pp. 553–606, http://dx.doi.org/10.1533/9780857097347.3.553.

[24] A.J. Jacobson, Materials for solid oxide fuel cells, Chem. Mater. (ISSN: 0897-4756) 22 (3) (2010) 660–674, http://dx.doi.org/10.1021/cm902640j.

[25] D.G. Cahill, Thermal conductivity measurement from 30 to 750 K: the 3w method, Rev. Sci. Instrum. (ISSN: 0034-6748) 61 (2) (1990) 802–808, http://dx.doi.org/10.1063/1.1141498.

[26] F. Yang, X. Zhao, P. Xiao, Thermal conductivities of YSZ/Al_2O_3 composites, J. Eur. Ceram. Soc. (ISSN: 09552219) 30 (15) (2010) 3111–3116, http://dx.doi.org/10.1016/j.jeurceramsoc.2010.07.007.

[27] R. Papitha, M. Suresh, D. Das, R. Johnson, Effect of micro-cracking on the thermal conductivity and thermal expansion of tialite (Al_2TiO_5) ceramics, Process. Appl. Ceram. (ISSN: 1820-6131) 7 (3) (2013) 143–146, http://dx.doi.org/10.2298/PAC1303143P.

[28] J. Hostaša, W. Pabst, J. Matějíček, Thermal conductivity of Al_2O_3-ZrO_2 composite ceramics, J. Am. Ceram. Soc. (ISSN: 00027820) 94 (12) (2011) 4404–4409, http://dx.doi.org/10.1111/j.1551-2916.2011.04875.x.

[29] L. Zhang, W. Pan, Structural and thermo-mechanical properties of Nd: y_2o_3 transparent ceramics, J. Am. Ceram. Soc. (ISSN: 00027820) 98 (10) (2015) 3326–3331, http://dx.doi.org/10.1111/jace.13735.

[30] H. Kellogg (Ed.), Applications of Fundamental Thermodyamics to Metallurgical Processes, Gordon and Breach, 1967.

[31] A. Mostafa, J.M. Eakman, S.L. Yarbro, Prediction of heat capacities of solid inorganic salts from group contributions, 1997, http://dx.doi.org/10.2172/426978.

[32] O. Kubaschewski, H. Ünal, An empirical estimation of the heat capacities of inorganic compounds, High Temp.–High Pressures (9) (1977) 361–365.

[33] R.G. Berman, T.H. Brown, Heat capacity of minerals in the system Na_2O-K_2O-CaO-MgO-FeO-Fe_2O_3-Al_2O_3-SiO_2-TiO_2-H_2O-CO_2: representation, estimation, and high temperature extrapolation, Contributions to Mineralogy and Petrology (89) (1985) 168–183.

[34] J. Leitner, P. Chuchvalec, D. Sedmidubsky, Estimation of heat capacities of binary oxides in the solid state, Chem. Listy 95 (1) (2001).

[35] J. Leitner, P. Chuchvalec, D. Sedmidubský, A. Strejc, P. Abrman, Estimation of heat capacities of solid mixed oxides, Thermochim. Acta (ISSN: 00406031) 395 (1–2) (2002) 27–46, http://dx.doi.org/10.1016/S0040-6031(02)00177-6.

[36] W. Wang, X. Chen, Y. Chen, Y. Dong, C. Ma, Calculation and verification for the thermodynamic data of $3CaO \cdot 3Al_2O_3 \cdot CaSO_4$, Chin. J. Chem. Eng. (ISSN: 10049541) 19 (3) (2011) 489–495, http://dx.doi.org/10.1016/S1004-9541(11)60011-6.

[37] M. Chase, NIST-JANAF Thermochemical Tables, 4th Edition, American Institute of Physics, -1, 1998.

[38] D.G. Archer, Thermodynamic properties of synthetic sapphire (α-al2o3), standard reference material 720 and the effect of temperature–scale differences on thermodynamic properties, J. Phys. Chem. Ref. Data (ISSN: 0047-2689) 22 (6) (1993) 1441–1453, http://dx.doi.org/10.1063/1.555931.

[39] D.S. Tsagareishvili, T.S. Yashvili, G.G. Gvelesiani, Enthalpy and heat capacity of scandium sesquioxide at high temperatures, Soobshch. Akad. Nauk Gruz. SSR 49 (1968) 175–180, https://www.osti.gov/biblio/4513509.

[40] U. Kolitsch, Hochtemperaturkalorimetrie und Phasenanalytik in SE_2O_3-Al_2O_3-SiO_2-Systemen (Ph.D. thesis), Inst. für Nichtmetallische Anorganische Materialien, 1995.

[41] Y. Zhang, I.-H. Jung, Critical evaluation of thermodynamic properties of rare earth sesquioxides (RE=La, Ce, Pr, Nd, Pm, Sm, Eu, Gd, Tb, Dy, Ho, Er, Tm, Yb, Lu, Sc and Y), CALPHAD (ISSN: 03645916) 58 (2017) 169–203, http://dx.doi.org/10.1016/j.calphad.2017.07.001.

[42] M. Zinkevich, Thermodynamics of rare earth sesquioxides, Prog. Mater. Sci. (ISSN: 00796425) 52 (4) (2007) 597–647, http://dx.doi.org/10.1016/j.pmatsci.2006.09.002.

[43] J. Manara, M. Arduini-Schuster, H.-J. Rätzer-Scheibe, U. Schulz, Infrared-optical properties and heat transfer coefficients of semitransparent thermal barrier coatings, Surf. Coat. Technol. (ISSN: 02578972) 203 (8) (2009) 1059–1068, http://dx.doi.org/10.1016/j.surfcoat.2008.09.033.

[44] J. Manara, Infrarot-optischer Strahlungstransport zur Analyse der Struktur und der Wärmeleitfähigkeit von Keramiken für Hochtemperaturanwendungen: Dissertation zur Erlangung des naturwissenschaftlichen Doktorgrades der Bayerischen Julius-Maximilians- Universität Würzburg, 2001.

[45] L.A. Dombrovsky, B. Rousseau, P. Echegut, J.H. Randrianalisoa, D. Baillis, High temperature infrared properties of YSZ electrolyte ceramics for SOFCs: Experimental determination and theoretical modeling, J. Am. Ceram. Soc. (ISSN: 00027820) 94 (12) (2011) 4310–4316, http://dx.doi.org/10.1111/j.1551-2916.2011.04655.x.

[46] J.I. Eldridge, C.M. Spuckler, Determination of scattering and absorption coefficients for plasma-sprayed yttria-stabilized zirconia thermal barrier coatings, J. Am. Ceram. Soc. (ISSN: 00027820) 91 (5) (2008) 1603–1611, http://dx.doi.org/10.1111/j.1551-2916.2008.02349.x.

[47] K. Nakazawa, A. Ohnishi, Simultaneous measurement method of normal spectral emissivity and optical constants of solids at high temperature in vacuum, Int. J. Thermophys. (ISSN: 0195-928X) 31 (10) (2010) 2010–2018, http://dx.doi.org/10.1007/s10765-010-0847-0.

[48] Q. Cheng, P. Yang, Z. Zhang, Radiative properties of ceramic Al_2O_3, AlN, and Si_3N_4: I. experiments, Int. J. Thermophys. (ISSN: 0195-928X) 37 (6) (2016) http://dx.doi.org/10.1007/s10765-016-2067-8.

[49] D.A. Permin, A.V. Belyaev, S.S. Balabanov, V.A. Koshkin, M.S. Boldin, A.V. Novikova, O.V. Timofeev, Z.K. Gashpar, I.V. Ladenkov, Effect of composition on the structure and properties of mgo/y_2o_3 composite ceramics, Inorgan. Mater. (ISSN: 0020-1685) 58 (6) (2022) 643–650, http://dx.doi.org/10.1134/S0020168522060085.

[50] N. Arifin, T. Button, R. Steinberger-Wilckens, Carbon-tolerant Ni/ScCeSZ via aqueous tape casting for IT- SOFCs, ECS Trans. (ISSN: 1938-6737) 78 (1) (2017) 1417–1425, http://dx.doi.org/10.1149/07801.1417ecst.

[51] J. Neutzler, X. Huang, J. Sightler, Y. Chen, N. Orlovskaya, High conductivity solid oxide electrolyte composite-laminates utilizing scandia/ceria co-doped zirconia core with yttria stabilized zirconia outer skins, 2011, http://dx.doi.org/10.13140/RG.2.2.19516.95361.

[52] K. Yang, J.X. Wang, Y.J. Xue, M.S. Wang, C.R. He, Q. Wang, H. Miao, W.G. Wang, Synthesis, sintering behavior and electrical properties of $Ba(Zr0.1Ce0.7Y0.2)O_{3-\delta}$ and $Ba(Zr0.1Ce0.7Y0.1Yb0.1)O_{3-\delta}$ proton conductors, Ceram. Int. (ISSN: 02728842) 40 (9) (2014) 15073–15081, http://dx.doi.org/10.1016/j.ceramint.2014.06.115.

[53] S. Raghavan, H. Wang, R.B. Dinwiddie, W.D. Porter, M.J. Mayo, The effect of grain size, porosity and yttria content on the thermal conductivity of nanocrystalline zirconia, Scr. Mater. (ISSN: 13596462) 39 (8) (1998) 1119–1125, http://dx.doi.org/10.1016/S1359-6462(98)00290-5.

[54] K. Sasaki, T. Terai, A. Suzuki, N. Akasaka, Effect of the Y_2O_3 concentration in YSZ on the thermophysical property as a thermal shielding material, Int. J. Appl. Ceram. Technol. (ISSN: 1546542X) (2009) http://dx.doi.org/10.1111/j.1744-7402.2009.02363.x.

[55] J. Yang, Y. Han, M. Shahid, W. Pan, M. Zhao, W. Wu, C. Wan, A promising material for thermal barrier coating: Pyrochlore-related compound Sm_2FeTaO_7, Scr. Mater. (ISSN: 13596462) 149 (2018) 49–52, http://dx.doi.org/10.1016/j.scriptamat.2018.02.005.